A micro-mechanical homogenisation model for masonry:

Application to shear walls

A. ZUCCHINI *
ENEA, FIM-FIS.MET, C.R.E. "E.Clementel", v. Martiri di Montesole, 4 , I – 40129 Bologna, Italy.

E-mail: zucchini@bologna.enea.it,Ph: +39 0516098256, Fax: +39 0516098062

P.B. LOURENÇO
University of Minho, Department of Civil Engineering, Azurém, P – 4800-058 Guimarães, Portugal

E-mail: pbl@civil.uminho.pt, Ph: + 351 253 510200, Fax: + 351 253 510217

* Corresponding author

ABSTRACT

An improved micro-mechanical model for masonry homogenisation in the non linear domain, is proposed and validated by comparison with experimental and numerical results available in the literature. Suitably chosen deformation mechanisms, coupled with damage and plasticity models, can simulate the behaviour of a basic periodic cell up to complete degradation and failure. The micro-mechanical model can be implemented in any standard finite element program as a user supplied subroutine defining the mechanical behaviour of an equivalent homogenised material. This work shows that, with the proposed model, it is possible to capture and reproduce the fundamental features of a masonry shear wall up to collapse with a coarse finite element mesh. The main advantage of such homogenisation approach is obviously the possibility to simulate real complex structures while taking into consideration the arrangement of units and mortar, which would otherwise require impractical amount of finite elements and computer resources.

KEYWORDS

Masonry; Macro-modelling; Homogenisation; Plasticity; Damage.

1. Introduction

Masonry is a heterogeneous material that consists of units and joints. The huge number of possible combinations generated by the geometry, nature and arrangement of units as well as the characteristics of mortars raises doubts about the accuracy of the term “masonry”. Still, it is certain that the arrangement of the masonry units (masonry bond or texture) and the components have much influence on the properties of the composite. A first good example is given in Lourenco and Ramos (2004), where the shear strength of dry masonry joints is tested. It is shown that the surface treatment of the masonry units, while keeping the same material, affects not only the strength of the joint but also its dilatancy under cyclic loading. A second good example is given in Vasconcelos (2005) where stone masonry shear walls are tested under cyclic loading, keeping the component materials while changing the masonry bond. It is demonstrated that significant changes occur in the response in terms of strength and stiffness degradation, energy dissipation and force-displacement diagrams.

Thus, masonry is a material exhibiting distinct directional properties due to the mortar joints, which act as planes of weakness. Depending on the level of accuracy and simplicity desired, it is possible to use different modelling strategies. The possibilities of structural analysis of masonry structures have been addressed e.g. in Lourenco and Ramos (2004), where it is advocated that most techniques of analysis are adequate, possibly for different applications, if combined with proper engineering reasoning, while recent advances in terms of sophisticated analysis homogenisation tools are discussed in Lourenco et al. (2007). Recent works in the non-linear field include, for example, the polynomial stress field expansion approach of Milani et al. (2006) and the mesoscopic approached of Massart et al. (2004), Calderini and Lagomarsino (2006), and Shieh-Beygia and Pietruszczak

(2008).

Homogenisation techniques (Fig. 1), which permit to establish constitutive relations in terms of averaged stresses and strains from the geometry and constitutive relations of the individual components, can represent a step forward in masonry modelling, mostly because of the possibility to use standard material models and software codes for isotropic materials. Despite the complexity of masonry, much information can be gained from the study of regular masonry structures, in which a periodic repetition of the microstructure occurs due to a constant arrangement of the units (or constant bond). Here, attention is given to a micromechanical homogenisation model that incorporates suitably chosen deformation mechanisms. Traditionally, experiments on shear walls have been adopted by the masonry community as the most common in-plane large test for validating advanced simulations and understanding masonry failure. It will be shown that the proposed model is capable of reproducing well such experimental results available in the literature.

2. Formulation of the model

2.1. General

Zucchini and Lourenço (2002) have shown that the elastic mechanical properties of an orthotropic material equivalent to a basic masonry cell can be derived from a suitable micromechanical model with appropriate deformation mechanisms, which take into account the staggered alignment of the units in a masonry wall. The unknown internal stresses and strains can be found from equilibrium equations at the interfaces between the basic cell components, from a few ingenuous assumptions on the kinematics of the basic cell deformation and by forcing the macro-deformations of the model and of the homogeneous material to

contain the same strain energy. This homogenisation model has already been extended with good results to non-linear problems in the case of a masonry cell failure under tensile loading parallel to the bed joint (Zucchini and Lourenço, 2004) or under compressive loading perpendicular to the bed joint (Zucchini and Lourenço, 2007). The simulations have been accomplished by coupling the elastic micro-mechanical model with a damage model in tension and a plasticity model in compression by means of an iterative solution procedure to calculate respectively the damage coefficients and the plastic strains in joints and units. The micromechanical model was based on a quarter of the periodic basic cell in running bond masonry shown in Fig. 2. This approach implies symmetry conditions at the boundary of the basic cell, what is true as far as shear loads are not present. In previous validation tests this requirement was satisfied, because the basic cell was loaded only with normal stresses.

According to the basic shear mechanism described in Zucchini and Lourenço (2002), the vertical elastic stress in the bed joints of two neighbouring quarter cells, under plain shear, is of opposite sign, due to the intrinsic antisymmetry of shear loads. Application of the homogenisation model to real mixed loading conditions of generic masonry cells needs therefore to take into account such antisymmetry, which can lead to differentiated failure or material degradation of symmetric bed joints. The simulation of non linear shear deformation requires the extension of the micromechanical model to a full periodic cell and the introduction of new antisymmetric deformation mechanisms of masonry with two distinct antisymmetric bed joints. In the improved model, as it will be described in the following sections, the main consequence in the mechanics of the deformation is the behaviour of the head joint : its shear deformation under normal loads and horizontal deformation under shear loads, absent in the previous quarter cell

model, have now to be taken into account. The geometry of the full masonry cell and its components are shown in Fig. 2, where it can be seen that the complex internal structure is represented by only five different components, namely units (component b), two antisymmetric bed joints (components 1A and 1B), head joints (component 2) and cross joints (component 3).

2.2. Quarter cell formulation

When the basic cell is loaded only with normal stresses, the micromechanical model of Zucchini and Lourenço (2002) assumes that all shear stresses and strains inside the basic cell can be neglected, with the exception of the in-plane shear stress and strain (σ_{xy} and ε_{xy}) in the bed joint and in the unit. The non-zero stresses and strains in the bed joint, head joint and unit are assumed to be constant, with the exception of the normal stress σ_{xx} in the unit, which is a linear function of x and accounts for the effect of the shear σ_{xy} in the bed joint, and with the exception of the shear stress σ_{xy} in the unit, which is linear in y.

The coupling of this model with a material damage model in tension (Zucchini and Lourenço, 2004) and a Drucker-Prager plasticity model in compression (Zucchini and Lourenço, 2007) leads, for each homogenized strain increment $\Delta\boldsymbol{\varepsilon}^0$, to an iterative algorithm, shown in Fig. 3, in which at each iteration a system of equilibrium equations is solved to obtain the unknown internal stresses(σ_j^i) and strains (ε_j^i) in the cell components (i=1A,1B,2,3,b), making use of the damage coefficients and of the plastic strains from the previous iteration. The superscript ^{0} is used for homogenized cell variables. Both the damage coefficients and the plastic strains are then updated, by means of the damage and plasticity models, respectively from the new stresses and from the

new total strains and the process is iterated until convergence of the stresses, within an input tolerance. Finally, the damaged internal stresses in the cell components and the unknown homogenised stresses $\boldsymbol{\sigma}^0$ can be derived from the values of the converged internal stresses.

The governing linear system of 20 equilibrium equations in the unknown internal stresses and total strains of a masonry cell, to be solved at each iteration for a quarter cell geometry under normal strains in *x* and *y* and null normal stress in *z*, is (Zucchini and Lourenço, 2007) :

(1) $$r^2\sigma_{xx}^2 = r^b\bar{\sigma}_{xx}^b - \frac{l-t}{2h}r^1\sigma_{xy}^1$$ Interface brick-head joint

(2) $$r^b\sigma_{yy}^b = r^1\sigma_{yy}^1$$ Interface brick-bed joint

(3) $$(l-t+2t\frac{r^1}{r^3})\varepsilon_{xx}^1 = (l+t)\varepsilon_{xx}^0$$ Right boundary

(4) $$(h+2t\frac{r^2}{r^3})\varepsilon_{yy}^2 + h\varepsilon_{yy}^b = 2(h+t)\varepsilon_{yy}^0$$ Upper boundary

(5) $$thr^2\sigma_{zz}^2 + (l-t+2t\frac{r^3}{r^1})tr^1\sigma_{zz}^1 + lhr^b\sigma_{zz}^b = 0$$ Front boundary

(6) $$2t\varepsilon_{yy}^1 + h\varepsilon_{yy}^b = (2t\frac{r^2}{r^3} + h)\varepsilon_{yy}^2$$ Upper boundary

(7) $$t\varepsilon_{xx}^2 + l\bar{\varepsilon}_{xx}^b = (l-t+2t\frac{r^1}{r^3})\varepsilon_{xx}^1$$ Right boundary

(8) $$\varepsilon_{zz}^b = \varepsilon_{zz}^1$$ Front boundary

(9) $$\varepsilon_{zz}^b = \varepsilon_{zz}^2$$ Front boundary

(10)
$$\varepsilon_{xx}^k = \frac{1}{E_k}\left[\sigma_{xx}^k - \nu_k\left(\sigma_{yy}^k + \sigma_{zz}^k\right)\right] + \varepsilon_{p,xx}^k$$
$$\varepsilon_{yy}^k = \frac{1}{E_k}\left[\sigma_{yy}^k - \nu_k\left(\sigma_{xx}^k + \sigma_{zz}^k\right)\right] + \varepsilon_{p,yy}^k \qquad k = b,1,2$$
$$\varepsilon_{zz}^k = \frac{1}{E_k}\left[\sigma_{zz}^k - \nu_k\left(\sigma_{xx}^k + \sigma_{yy}^k\right)\right] + \varepsilon_{p,zz}^k$$

(11) $$\varepsilon_{xy}^{1} = \frac{\varepsilon_{xx}^{2} - \bar{\varepsilon}_{xx}^{b}}{4} - \left(\frac{l-t}{8hE^{b}} + \frac{h}{6tG^{b}}\right)\frac{r^{1}}{r^{b}}\sigma_{xy}^{1}$$

(12) $$\sigma_{xy}^{1} = 2G^{1}\left(\varepsilon_{xy}^{1} - \varepsilon_{p,xy}^{1}\right)$$

The above system has been obtained with the following assumptions concerning the cross joint :

(13) $$\varepsilon_{yy}^{3} = \frac{r_2}{r_3}\varepsilon_{yy}^{2} \quad , \quad \varepsilon_{xx}^{3} = \frac{r_1}{r_3}\varepsilon_{xx}^{1} \quad , \quad \sigma_{zz}^{3} = \sigma_{zz}^{1} \quad , \quad \sigma_{xx}^{3} = \frac{r_1}{r_3}\sigma_{xx}^{1}$$

Eqs.(13a-b) assume respectively that the cross joint behaves as a spring connected in series with the bed joint in the *x*-direction and connected in parallel with the bed joint in the *z*-direction.

As shown in Fig. 2, *l* is half of the unit length, *h* is half of the unit height and *t* is half of the bed joint width. Here also, *E* is the Young modulus, *G* is the shear modulus, ν is the Poisson coefficient, $\boldsymbol{\varepsilon}, \boldsymbol{\varepsilon}_p$ and $\boldsymbol{\sigma}$ are the total strain, plastic strain and stress tensors. Unit, bed joints, head joint and cross joint variables are indicated throughout this paper, respectively by the superscripts *b*, 1 (1A and 1B for the full cell), 2 and 3, according to Fig. 2. $\bar{\sigma}_{xx}^{b}$ and $\bar{\varepsilon}_{xx}^{b}$ are the mean value of the (non-constant) normal stress σ_{xx} and of the (non-constant) normal strain ε_{xx} in the unit, respectively. ε_{xx}^{0} and ε_{yy}^{0} are the uniform normal (macro) strains on the faces of the homogenised basic cell. Finally, $r = 1 - d$, where *d* is the scalar damage coefficient, ranging from 0 to 1 and representing a measure of the material damage. The unknown damage of the cross joint in the above equation system has been assumed to be :

(14) $$r^{3} = \frac{r^{1} + r^{2}}{2}$$

The adopted damage model in tension (Zucchini and Lourenço, 2004) is a simple scalar isotropic model, with a Rankine type damage surface, where the

damage can only increase monotonically with an exponential evolution law. A non-associated Drucker-Prager model (Zucchini and Lourenço, 2007) has been adopted for the simulation of the plastic deformation of the cell components. The unknown plastic strains $\boldsymbol{\varepsilon}_p$ of the Drucker-Prager model are assumed to be constant in each cell component and are derived from the total strains $\boldsymbol{\varepsilon}$ with a return mapping algorithm, i.e. by integration over the loading path of a system of incremental elasto-plastic equations. With the plastic model it has been possible to take into account the degradation of the mechanical properties of the quarter cell components due not only to damage in tension, but also to plastic flow and hardening-softening of current material strengths with increasing deformations.

2.3. Full cell under normal loads: $\varepsilon_{xx}^0, \varepsilon_{yy}^0, \sigma_{zz}^0 = 0$

As mentioned in Section 2.1, shear loads induce an internal antisymmetric deformation of masonry periodic cells, where neighbouring quarter cells can develop different material damages and plastic deformations. Therefore, the homogenisation model based on a periodic quarter cell can no longer be used when shear is involved and the formulation must be extended to a full masonry cell. The missing mechanism in normal loading conditions is shown in Fig. 4 : if the non linear material properties of bed joints 1A and 1B evolve differently due to shear, the vertical displacements of the bricks in the middle of the cell are no longer equal, but antisymmetric. Taking into account the presence in the cell of two different bed joints (designated respectively as 1A and 1B), the equilibrium equations (1)-(12) for the full cell can now be rewritten as :

(15) $$r^2\sigma_{xx}^2 = r^b\overline{\sigma}_{xx}^b + \frac{l-t}{2h}\left(\frac{r^{1B}\sigma_{xy}^{1B} - r^{1A}\sigma_{xy}^{1A}}{2}\right)$$ Interface brick-head joint

(16) $$r^b\sigma_{yy}^b = \frac{r^{1A}\sigma_{yy}^{1A} + r^{1B}\sigma_{yy}^{1B}}{2}$$ Interface brick-bed joint

(17) $$(l-t+2t\frac{r^{1A}}{r^3})\varepsilon_{xx}^{1A} + (l-t+2t\frac{r^{1B}}{r^3})\varepsilon_{xx}^{1B} = 2(l+t)\varepsilon_{xx}^0$$ Right boundary

(18) $$(h+2t\frac{r^2}{r^3})\varepsilon_{yy}^2 + h\varepsilon_{yy}^b = 2(h+t)\varepsilon_{yy}^0$$ Upper boundary

(19) $$2thr^2\sigma_{zz}^2 + (l-t+2t\frac{r^3}{r^{1A}})tr^{1A}\sigma_{zz}^{1A} + (l-t+2t\frac{r^3}{r^{1B}})tr^{1B}\sigma_{zz}^{1B} + 2lhr^b\sigma_{zz}^b = 0$$

Front boundary

(20) $$t\left(\varepsilon_{yy}^{1A} + \varepsilon_{yy}^{1B}\right) + h\varepsilon_{yy}^b = (2t\frac{r^2}{r^3} + h)\varepsilon_{yy}^2$$ Upper boundary

(21) $$(l-t+2t\frac{r^{1A}}{r^3})\varepsilon_{xx}^{1A} + (l-t+2t\frac{r^{1B}}{r^3})\varepsilon_{xx}^{1B} = 2t\varepsilon_{xx}^2 + 2l\bar{\varepsilon}_{xx}^b$$ Right boundary

(22) $$\varepsilon_{zz}^b = \varepsilon_{zz}^{1A}$$ Front boundary

(23) $$\varepsilon_{zz}^b = \varepsilon_{zz}^2$$ Front boundary

(24)
$$\varepsilon_{xx}^k = \frac{1}{E_k}\left[\sigma_{xx}^k - \nu_k\left(\sigma_{yy}^k + \sigma_{zz}^k\right)\right] + \varepsilon_{p,xx}^k$$
$$\varepsilon_{yy}^k = \frac{1}{E_k}\left[\sigma_{yy}^k - \nu_k\left(\sigma_{xx}^k + \sigma_{zz}^k\right)\right] + \varepsilon_{p,yy}^k$$ k = 1A,1B,2,b
$$\varepsilon_{zz}^k = \frac{1}{E_k}\left[\sigma_{zz}^k - \nu_k\left(\sigma_{xx}^k + \sigma_{yy}^k\right)\right] + \varepsilon_{p,zz}^k$$

(25) $$\varepsilon_{xy}^{1A} = \frac{\varepsilon_{xx}^2 - \bar{\varepsilon}_{xx}^b}{4} - (\frac{l-t}{16hE_b} + \frac{h}{12tG_b})\frac{\left(r^{1A}\sigma_{xy}^{1A} - r^{1B}\sigma_{xy}^{1B}\right)}{r^b}$$

(26) $$\sigma_{xy}^k = 2G_k\left(\varepsilon_{xy}^k - \varepsilon_{p,xy}^k\right)$$ k = 1A,1B,2

Here the damage of the cross joint has been assumed to be:

(27) $$r^3 = \max\left(r^{1A}, r^{1B}, r^2\right)$$

instead of Eq.(14). Using the mean value of bed and head joints, when the bed joints are completely damaged but the later is still carrying load, the cross joint would keep some residual strength under vertical tension with unrealistic results.

Eqs.(13), which allow to eliminate the unknown cross joint variables, become now :

(28) $$\varepsilon_{yy}^{3} = \frac{r^{2}}{r^{3}}\varepsilon_{yy}^{2} \quad , \quad \varepsilon_{xx}^{3} = \frac{r^{1A}\varepsilon_{xx}^{1A} + r^{1B}\varepsilon_{xx}^{1B}}{2r^{3}}$$

(29) $$\sigma_{zz}^{3} = \frac{\sigma_{zz}^{1A} + \sigma_{zz}^{1B}}{2} \quad , \quad \sigma_{xx}^{3} = \frac{r^{1A}\sigma_{xx}^{1A} + r^{1B}\sigma_{xx}^{1B}}{2r^{3}}$$

With the distinction of two different bed joints, eight new variables (four strains and four stresses) have been added to the problem. Moreover the shear deformation of the head joint must now be included, with two additional unknowns. The shear deformation of the brick is neglected, even if it is taken partly into account with a correction term in Eq.(25), as described in Zucchini and Lourenço (2004). Additional equations are needed for the solution of the problem. The elastic stress-strain relations in Eqs.(24) for the new bed joint and the shear in Eq.(26) for the new bed joint and the head joint provide five new equations. In addition the deformation mechanism under normal loads assumes that :

(30) $$\varepsilon_{zz}^{1A} = \varepsilon_{zz}^{1B} \quad , \quad \varepsilon_{xy}^{1A} = -\varepsilon_{xy}^{1B} \quad , \quad \varepsilon_{xx}^{1A} = \varepsilon_{xx}^{1B}$$

A further equation is provided by the equilibrium of the bricks in the y-direction with symmetric boundary conditions at the boundaries of the full cell :

(31) $$2(l-t)r^{1A}\sigma_{yy}^{1A} - 2(l-t)r^{1B}\sigma_{yy}^{1B} + 4hr_{2}\sigma_{xy}^{2} = 0$$

The shear strain in the head joint, ε_{xy}^{2}, which did not appear in the quarter cell model, can be easily derived with geometric considerations from Fig. 4 :

(32) $$\varepsilon_{xy}^{2} = \frac{\Delta y}{4t} = \frac{\varepsilon_{y}^{1A} - \varepsilon_{y}^{1B}}{2}$$

Eqs.(15)-(26),(30)-(32) provide a system of 30 equations and 30 unknowns, which completely characterizes the elastic behaviour of the full cell under normal loads in the model. This system, as expected, reduces to the previous quarter cell

formulation, when the material properties of the two bed joints 1A and 1B are identical. The homogenized shear stress on the upper boundary of the full cell (Fig.4) is $\sigma_{xy}^{0,n} = \dfrac{tr^2\sigma_{xy}^2 - tr^2\sigma_{xy}^2 + 2lr^b\sigma_{xy}^b}{2(t+l)}$ due to symmetry conditions assumed at cell boundaries. The unit shear is neglected in the assumed deformation mode and that leads to $\sigma_{xy}^{0,n} = 0$.

2.4. Full cell under in-plane shear: $\sigma_{xx}^0 = \sigma_{yy}^0 = \sigma_{zz}^0 = 0$, ε_{xy}^0

The deformation mechanism of an elastic quarter cell under plain shear load, described in Zucchini and Lourenço (2002), is extended in this paper to a full masonry cell (Fig. 5) with material damage and plastic deformation. The main difference with the previous formulation is that the head joint is strained in the x-direction because of the different shear deformations of the antisymmetric bed joints inside the full cell. The normal stress and strain, σ_{xx}^2 and ε_{xx}^2, in the head joint, previously neglected, must be taken into account in the full cell model. The analysis of internal equilibrium and geometric compatibilities leads to the following equations :

(33) $$t\left(\varepsilon_{yy}^{1A} + \varepsilon_{yy}^{1B}\right) + h\varepsilon_{yy}^b = (2t\frac{r^2}{r^3} + h)\varepsilon_{yy}^2$$ Upper boundary

(34) $$2t\varepsilon_{xx}^2 + 2l\bar{\varepsilon}_{xx}^b = (l - t + 2t\frac{r^{1A}}{r^3})\varepsilon_{xx}^{1A} + (l - t + 2t\frac{r^{1B}}{r^3})\varepsilon_{xx}^{1B}$$ Right boundary

(35) $$r^b\bar{\sigma}_{xy}^b = \frac{r^{1A}\sigma_{xy}^{1A} + r^{1B}\sigma_{xy}^{1B}}{2}$$ Interface brick-bed joint

(36) $$2hr^2\sigma_{xy}^2 - 2hr^b\bar{\sigma}_{xy}^b = (l-t)\left(\frac{r^{1B}\sigma_{yy}^{1B} - r^{1A}\sigma_{yy}^{1A}}{2}\right)$$ Interface brick-head joint

(37) $$4hr^2\sigma_{xx}^2 + (l-t)\left(r^{1A}\sigma_{xy}^{1A} - r^{1B}\sigma_{xy}^{1B}\right) = 4hr^b\bar{\sigma}_{xx}^b$$ Interface brick-head joint

(38) $2r^b\sigma_{yy}^b = r^{1A}\sigma_{yy}^{1A} + r^{1B}\sigma_{yy}^{1B}$ Interface brick-bed joint

In the inelastic domain the usual stress-strain relations hold :

$$\varepsilon_{xx}^k = \frac{1}{E_k}\left[\sigma_{xx}^k - \nu_k\left(\sigma_{yy}^k + \sigma_{zz}^k\right)\right] + \varepsilon_{p,xx}^k$$

(39) $$\varepsilon_{yy}^k = \frac{1}{E_k}\left[\sigma_{yy}^k - \nu_k\left(\sigma_{xx}^k + \sigma_{zz}^k\right)\right] + \varepsilon_{p,yy}^k \qquad k = 1A,1B,2,b$$

$$\varepsilon_{zz}^k = \frac{1}{E_k}\left[\sigma_{zz}^k - \nu_k\left(\sigma_{xx}^k + \sigma_{yy}^k\right)\right] + \varepsilon_{p,zz}^k$$

(40) $\sigma_{xy}^k = 2G_k\left(\varepsilon_{xy}^k - \varepsilon_{p,xy}^k\right)$ $k = 1A,1B,2,b$

The deformation mechanism is characterized by the following assumptions :

(41) $\varepsilon_{xx}^{1A} = \varepsilon_{xx}^{1B}$

(42) $\varepsilon_{zz}^b = \varepsilon_{zz}^{1A} = \varepsilon_{zz}^{1B} = \varepsilon_{zz}^2$

The procedure described in Zucchini and Lourenço (2002) for a quarter cell can be applied to the full cell and with the notation of Fig. 5 it is easily seen that :

(43) $\varepsilon_{xy}^{1A} = \frac{1}{2}\left(\frac{\Delta_A}{2t} - \frac{\Delta y}{l}\right)$, $\varepsilon_{xy}^{1B} = \frac{1}{2}\left(\frac{\Delta_B}{2t} - \frac{\Delta y}{l}\right)$

(44) $\bar{\varepsilon}_{xy}^b = \frac{1}{2}\left(\frac{\Delta_U}{2h} - \frac{\Delta y}{l}\right)$, $\varepsilon_{xy}^2 = \frac{1}{2}\left(\frac{\Delta_U}{2h} + \frac{\Delta y}{t}\right)$

(45) $8(h+t)\varepsilon_{xy}^0 = 2\Delta_U + \Delta_A + \Delta_B$

With some manipulation, the above relations yield :

(46) $\varepsilon_{xy}^2 - \bar{\varepsilon}_{xy}^b = \frac{\left(\varepsilon_{yy}^{1A} - \varepsilon_{yy}^{1B}\right)}{2}$

(47) $\varepsilon_{xx}^2 = \frac{\Delta_A - \Delta_B}{2t} + \varepsilon_{xx}^b = 2\left(\varepsilon_{xy}^{1A} - \varepsilon_{xy}^{1B}\right) + \bar{\varepsilon}_{xx}^b$

(48) $2(h+t)(l+t)\varepsilon_{xy}^0 = 2h\left(l\bar{\varepsilon}_{xy}^b + t\varepsilon_{xy}^2\right) + t(l+t)\left(\varepsilon_{xy}^{1A} + \varepsilon_{xy}^{1B}\right) + t^2\left(\varepsilon_{yy}^{1A} - \varepsilon_{yy}^{1B}\right)$

Finally the cell boundary conditions $\sigma_{xx}^0 = \sigma_{yy}^0 = \sigma_{zz}^0 = 0$ are imposed to the plain shear deformation :

(49) $$hr^2\sigma_{xx}^2 + hr^b\bar{\sigma}_{xx}^b + t\left(r^{1A}\sigma_{xx}^{1A} + r^{1B}\sigma_{xx}^{1B}\right) - \frac{(l-t)}{4}\left(r^{1B}\sigma_{xy}^{1B} - r^{1A}\sigma_{xy}^{1A}\right) = 0$$

(50) $$tr^2\sigma_{yy}^2 + lr^b\sigma_{yy}^b = 0$$

(51) $$2thr^2\sigma_{zz}^2 + t(l - t + 2t\frac{r^3}{r^{1A}})r^{1A}\sigma_{zz}^{1A} + t(l - t + 2t\frac{r^3}{r^{1B}})r^{1B}\sigma_{zz}^{1B} + 2lhr^b\sigma_{zz}^b = 0$$

Eqs.(33)-(42),(46)-(51) form a system of 32 equations and 32 unknowns, which can be solved to obtain the average stresses and strains in each cell component for an elastic cell under plain shear load. The homogenised normal strains of the cell under in-plane shear can finally be evaluated as :

(52) $$\varepsilon_{xx}^{0,s} = \frac{t\varepsilon_{xx}^2 + l\bar{\varepsilon}_{xx}^b}{(t+l)}$$

(53) $$\varepsilon_{yy}^{0,s} = \frac{h}{(h+t)}\varepsilon_{yy}^b + \frac{t}{2(h+t)}\left(\varepsilon_{yy}^{1A} + \varepsilon_{yy}^{1B}\right)$$

2.5. Mixed in-plane loading conditions

Under in-plane loading the masonry cell experiences a combination of normal and in-plane shear deformations. The boundary conditions imposed to the cell are the total strains $\varepsilon_{xx}^0, \varepsilon_{yy}^0$ and ε_{xy}^0 with the plane stress constraint $\sigma_{zz}^0 = 0$, and the internal strains and stresses are calculated summing up the contributions due to the normal and shear loads imposed separately to the cell. Note that because the shear model generates the homogenised strains given by Eqs.(52),(53), the actual boundary conditions for the normal loads problem must be :

(54) $$\varepsilon_{xx}^{0,n} = \varepsilon_{xx}^0 - \varepsilon_{xx}^{0,s} \quad , \quad \varepsilon_{yy}^{0,n} = \varepsilon_{yy}^0 - \varepsilon_{yy}^{0,s}$$

for the total strains to be the required values.

The coupling of the two loading models is carried out assuming that the plastic deformation of each internal cell component is decomposed in two parts :

(55) $$\boldsymbol{\varepsilon}^{p,k} = \boldsymbol{\varepsilon}_n^{p,k} + \boldsymbol{\varepsilon}_s^{p,k} \qquad k = 1A,1B,2,b$$

where $\boldsymbol{\varepsilon}_n^{p,k}$ and $\boldsymbol{\varepsilon}_s^{p,k}$ are plastic strains conventionally ascribed respectively to the normal and shear loads. The stresses $\boldsymbol{\sigma}_n^k$ and the total strains $\boldsymbol{\varepsilon}_n^k$ in the cell under the normal loads are then obtained by solving the system described in Section 2.3, with the assumption that the only plastic strains present in the cell are the strains $\boldsymbol{\varepsilon}_n^{p,k}$. Similarly the cell shear deformation ($\boldsymbol{\sigma}_s^k$ and $\boldsymbol{\varepsilon}_s^k$) is given by the solution of the equation system provided in Section 2.4, taking into account only the plastic strains $\boldsymbol{\varepsilon}_s^{p,k}$ in this case. It is implicit in the proposed approach that the plastic deformation ascribed to one loading condition does not affect the other.

The final total strains and stresses inside the cell under mixed load can be obtained simply by summing up the results :

(56) $$\boldsymbol{\sigma}^k = \boldsymbol{\sigma}_n^k + \boldsymbol{\sigma}_s^k \quad , \quad \boldsymbol{\varepsilon}^k = \boldsymbol{\varepsilon}_n^k + \boldsymbol{\varepsilon}_s^k \qquad k = 1A,1B,2,b$$

This method has proven numerically to be quite effective. On the contrary spurious oscillations arise in the iterative solution of the elasto-plastic problem if the same total plastic strain is used in both loading conditions without decomposition in "normal" and "shear" contributions. These oscillations lead to slow convergence, if any. The decomposition of the plastic strain is carried out by means of an arbitrary but simple and intuitive assumption : the two components of plastic strain in Eq.(55) are defined as the accumulation of plastic strains increments proportional to shear stresses $\sigma_{xy,n}^k$ and $\sigma_{xy,s}^k$ respectively, as described in next section.

2.6. Plastic model

The study of the inelastic behaviour of the basic cell up to and after failure requires the introduction of a non-linear constitutive model for the simulation of

the plastic deformation of each cell component. In previous work (Zucchini and Lourenço, 2007) a complex Drucker-Prager model has been adopted. Here, a much simpler Mohr-Coulomb model will be used, to avoid the well known problems related to the apex region of the Drucker-Prager yield function. In addition, due to cell geometry, plastic shear flow in bed joints and bricks is restricted only to *x*-direction, and to *y*-direction in head joints. With these assumptions the Mohr-Coulomb friction criteria reads as :

$$f(\boldsymbol{\sigma}, \varepsilon_{p,eq}) = \left|\sigma_{xy}\right| + \sigma_n \tan\phi_f - c = 0 \tag{57}$$

where: $\sigma_n = \sigma_{yy}$ for bed joints and bricks, $\sigma_n = \sigma_{xx}$ for head joints. The friction angle ϕ_f and the cohesion c are a function of the equivalent plastic strain $\varepsilon_{p,eq}$. The unknown plastic strains $\boldsymbol{\varepsilon}_p$ are assumed to be constant in each cell component and can be derived from the total (elastic + plastic) strains $\boldsymbol{\varepsilon}$ by integration over the loading path of the following system of incremental elasto-plastic equations from stage *i*–1 to stage *i*, e.g. Lourenço (1996) :

$$\begin{cases} \boldsymbol{\sigma}^i = \boldsymbol{\sigma}^* - \mathbf{D}\Delta\boldsymbol{\varepsilon}_p^i & \textit{plastic corrector} \\ \Delta\boldsymbol{\varepsilon}_p^i = \Delta\lambda^i \dfrac{\partial g(\boldsymbol{\sigma}^i, \varepsilon_{p,eq}^i)}{\partial \boldsymbol{\sigma}^n} & \textit{flow rule} \\ f(\boldsymbol{\sigma}^i, \varepsilon_{p,eq}^i) = t^i - p^i \tan\phi_f(\varepsilon_{p,eq}^i) - c(\varepsilon_{p,eq}^i) = 0 & \textit{yield surface} \end{cases} \tag{58}$$

Here, as in Zucchini and Lourenço (2007), the vector notation for stress and strains is used, being **D** the elastic stiffness matrix, $\boldsymbol{\sigma}^*$ the elastic predictor

$$\boldsymbol{\sigma}^* = \boldsymbol{\sigma}^{i-1} + \mathbf{D}\Delta\boldsymbol{\varepsilon}^i \tag{59}$$

$t = \dfrac{3 - \sin\phi_f}{6\cos\phi_f} q$ a deviatoric stress measure, q the equivalent stress, p the hydrostatic stress, g the non-associated plastic potential

$$g(\boldsymbol{\sigma}, \varepsilon_{p,eq}) = f\left(\varepsilon_{eq}\right) = \left|\sigma_{xy}\right| + \sigma_n \tan\phi_d - c \tag{60}$$

in general with a dilatancy angle $\phi_d \neq \phi_f$, and finally $\varepsilon^i_{p,eq}$ is the equivalent plastic strain, given by

(61) $$\Delta\varepsilon^i_{p,eq} = \sqrt{\frac{2}{3}(\Delta\bar{\boldsymbol{\varepsilon}}^i_p)^T(\Delta\bar{\boldsymbol{\varepsilon}}^i_p)}$$

where the notation $\bar{\boldsymbol{\varepsilon}}_p$ means the vector $\bar{\boldsymbol{\varepsilon}}^T_p = \left\{\varepsilon_{p1},\varepsilon_{p2},\varepsilon_{p3},\sqrt{2}\varepsilon_{p4},\sqrt{2}\varepsilon_{p5},\sqrt{2}\varepsilon_{p6}\right\}$.

Now, combining Eq.(58b) and Eq.(60) results in

(62) $$\left(\Delta\boldsymbol{\varepsilon}^i_p\right)^T = \Delta\lambda^i\,\mathbf{d}^T = \Delta\lambda^i\left\{0,\tan\phi_d,0,\pm1,0,0\right\}$$

and the equivalent plastic strain increment can be derived from Eqs.(61),(62) :

(63) $$\Delta\varepsilon^i_{p,eq} = \Delta\lambda^i\sqrt{\frac{2}{3}\left(\tan^2\phi_d + 2\right)}$$

The stress state in each loading step, when plasticity is active, must lie on the Coulomb yield surface, Eq.(58c). $\boldsymbol{\sigma}^i$ can be expressed through Eq.(58a), (60), (62) in terms of $\boldsymbol{\sigma}^{i-1}$, known from the previous converged loading step, $\Delta\boldsymbol{\varepsilon}^i$, the input strain increments during the current step, and the unknown plastic multiplier $\Delta\lambda^i$. Substituting $\sigma^i_{yy}(\boldsymbol{\sigma}^{i-1},\Delta\boldsymbol{\varepsilon}^i,\Delta\lambda^i)$ and $\sigma^i_{xy}(\boldsymbol{\sigma}^{i-1},\Delta\boldsymbol{\varepsilon}^i,\Delta\lambda^i)$ into Eq.(58c) leads to the equation in $\Delta\lambda^i$:

(64) $$c_1(\boldsymbol{\sigma}^{i-1},\Delta\boldsymbol{\varepsilon}i,\varepsilon^i_{p,eq})\Delta\lambda + c_2(\boldsymbol{\sigma}^{i-1},\Delta\boldsymbol{\varepsilon}^i,\varepsilon^i_{p,eq}) = 0$$

This equation is non linear because in general the coefficients c_1 and c_2 depend on the equivalent plastic strain $\varepsilon_{p,eq}$ through the friction angle ϕ_f and the cohesion c. If no strain hardening-softening is present, the coefficients $c_{1,2}(\sigma_{n-1},\Delta\boldsymbol{\varepsilon}^i_t)$ are known and constant in each loading step and Eq.(64) can be solved directly, otherwise the Newton-Raphson method is used for its solution. In this paper the friction angle is assumed to be independent from the plastic deformation, while an exponential law in $\varepsilon_{p,eq}$ is adopted for the material cohesion c:

(65) $$c = c_0 \exp\left(-\frac{c_0 \varepsilon_{p,eq}}{g^{II}} \right)$$

with c_0 the initial cohesion and g^{II} the specific mode II fracture energy :

The derivative $\frac{\partial c}{\partial \Delta\lambda} = \frac{\partial c}{\partial \varepsilon^i_{p,eq}} \frac{\partial \varepsilon^i_{p,eq}}{\partial \Delta\lambda}$, required for the iterative solution of Eq.(64), can be easily obtained by means of Eq.(63) :

(66) $$\frac{\partial c}{\partial \Delta\lambda} = -\frac{c_0}{g^{II}} c \sqrt{\frac{2}{3}\left(\tan^2 \phi_d + 2\right)}$$

Once the plastic multiplier $\Delta\lambda^i$ is obtained, the increments of plastic strains can be derived by Eq.(62), the new stresses can be obtained by Eq.(58a), and the equivalent plastic strain can be updated with Eq.(63) for the next loading step.

The plastic strains in the cell are decomposed in two components, Eq.(55), assumed to be the contributions of normal and shear loads respectively to the total plastic deformations. For sake of simplicity these terms are defined as separate accumulations of the plastic increments :

(67) $$\Delta\boldsymbol{\varepsilon}^{p,k}_n = t_n \Delta\boldsymbol{\varepsilon}^{p,k} \quad , \quad \Delta\boldsymbol{\varepsilon}^{p,k}_s = (1 - t_n)\Delta\boldsymbol{\varepsilon}^{p,k} \qquad k = 1\text{A},1\text{B},2,\text{b}$$

where the coefficient t_n is set to :

(68) $$t_n = \frac{|\sigma_{xy}| + |\sigma^n_{xy}| - |\sigma^s_{xy}|}{2|\sigma_{xy}|}$$

This function assigns the entire plastic strain to the component corresponding to the higher modulus, when σ^n_{xy} and σ^s_{xy} have different sign, otherwise the strain is distributed proportionally to the shear stress ratios $\frac{\sigma^n_{xy}}{\sigma_{xy}}$ and $\frac{\sigma^s_{xy}}{\sigma_{xy}}$.

2.7. Damage model : tension and compression

In Zucchini and Lourenco (2004) the micromechanical model for the quarter cell model has been coupled with a damage mechanics model to simulate the inelastic deformation of masonry in normal tension or compression. Continuum damage mechanics allows an effective simulation of the progressive deterioration of the mechanical properties, under increasing loading, in quasi-brittle materials such as concrete, rocks and masonry. The dissipative effects of micro-cracking in the material are taken into account by means of internal state variables, which affect the material strength and stiffness. Because the three-dimensional micromechanical model attempts to simulate the discrete internal structure of the basic cell, and implicitly the global anisotropic behaviour, the individual damage in each homogeneous isotropic component (joint or unit) has been taken into account. The advantage of this approach is that, for each component, an isotropic scalar damage model, with a single parameter, can be utilised, with obvious gains in simplicity and easiness of implementation.

The same approach used in Zucchini and Lourenço (2004) has been followed here, but with an important modification to account for large plastic deformations. A compressive damage based on a cap model has also been added to control masonry failure under high compressive loads. For each component of the full cell, both tension and compression models consists of :

a) *Scalar damage model*

The damaged $\boldsymbol{\sigma}_d$ and undamaged $\boldsymbol{\sigma}$ (or effective) stress tensors are correlated, according to continuum damage mechanics, by the relation:

(69) $$\boldsymbol{\sigma}_d = (1-d)\mathbf{D}\boldsymbol{\varepsilon} = (1-d)\boldsymbol{\sigma}$$

b) *Limit damage surface*

The limit damage surface is given by

(70) $\bar{\sigma} = \sigma_l$

where $\bar{\sigma}$ is the equivalent effective stress, a scalar function of the undamaged stress, and $\sigma_l = \sigma_t$ in tension, $\sigma_l = \sigma_c$ in compression, with σ_t and σ_c the material strengths in normal tension and compression of the given cell component.

c) *Equivalent effective stress*

The equivalent effective stress is defined as :

(71) $\bar{\sigma} = \sigma_n$ (Rankine criteria)

in normal tension, with σ_n the normal stress, and

(72) $\bar{\sigma} = \sqrt{\sigma_n^2 + \alpha\sigma_{xy}^2}$ (Compression cap)

in normal compression. To simplify the formulation, the following assumptions can be adopted for usual masonry, with units of higher strength than mortar :

a) bed joints can fail only in the y-direction : $\sigma_n = \sigma_{yy}$

b) head joints can fail only in the x-direction : $\sigma_n = \sigma_{xx}$

c) bricks can fail only in tension and in the x-direction : $\sigma_n = \sigma_{xx}$.

Failure of the brick in tension leads to a vertical localized crack which does not affect the capability of the brick to carry vertical load or shear. In the brick the damage coefficient is therefore actually applied in Eq.(69) only to the horizontal stress σ_{xx}^b, while d=0 is assumed for the others components .

d) *Damage evolution law*

The damage law for concrete-like materials adopted in Zucchini and Lourenço (2004) is :

(73) $d = 1 - \frac{\sigma_l}{\bar{\sigma}} \exp\left\{ A\left(1 - \frac{\bar{\sigma}}{\sigma_l} \right) \right\}$ $\sigma_l \le \bar{\sigma} \le \infty$

where *A* is a parameter chosen to reproduce the observed experimental behaviour.

This basic model has limitations in case of large plastic deformations. As clearly stated in Ju (1989), a stress based damage criterion, in presence of significant plastic flows, is inherently inadequate for predicting realistic plastic damage growth. For example, in perfect plasticity coupled with damage, a stress based criterion will not predict significant damage accumulation even under large plastic deformations. To avoid this problem the following modified damage evolution law has been adopted :

$$d = 1 - \frac{\sigma_l}{\bar{\sigma}} \exp\left\{ A\left(1 - \frac{E\bar{\varepsilon}}{\sigma_l} \right) \right\} \qquad \sigma_l \le \bar{\sigma} \le \infty \tag{74}$$

where $\bar{\varepsilon}$ is a suitable equivalent strain measure. In this way the damage increases monotonically with the deformation of the material, even if the stress is constant. Furthermore, because it is expected that the damage depends more on the tensile (compressive) deformations in normal tension (compression) than on the compressive (tensile) strains, the following definition of the equivalent strain for tensile damage (Mazars and Pijaudier-Cabot, 1989; Peerlings et al.,1998) has been used :

$$\bar{\varepsilon} = \sqrt{\sum_{i=1}^{3} \langle \varepsilon_i \rangle^2} \tag{75}$$

with ε_i, i=1, 2, 3, the principal tensile strains and $\langle ... \rangle$ the McAuley brackets. The dependence on solely the positive principal strains renders the equivalent strain more sensitive to tensile strains than to compressive strains. This definition has been implemented in the model, in incremental form, as follows :

$$\Delta\bar{\varepsilon}_t = \begin{cases} \sqrt{\sum_{i=1}^{3} \langle \Delta\varepsilon_i \rangle^2} & \text{if} \quad \bar{\sigma} \ge \sigma_l \\ \Delta\bar{\sigma} / E & \text{if} \quad \bar{\sigma} \le \sigma_l \end{cases} \tag{76}$$

for material damage in normal tension. For compression damage the positive tensile strain increments $\langle \Delta\varepsilon_i \rangle^2$ are replaced by the negative compression strain

increments $\langle -\Delta\varepsilon_i \rangle^2$. The incremental approach is valid as far as no reverse loading is present. The irreversibility of the damage process is accounted for by updating the damage coefficient only for increasing values, while the damage coefficients d_t and d_c due to normal tension and compression are calculated independently and only the maximum is applied to the effective stress :

(77) $$d' = \max\left(d, d_t, d_c\right).$$

e) *Correlation with fracture parameters*

In Zucchini and Lourenço (2004) it is shown that the damage model parameter A can be related to the specific mode I fracture energies in tension and compression, g_t^I and g_c^I (N/m^2), of the material by

(78) $$A_t = \left(\frac{g_t^I E}{\sigma_t^2} - \frac{1}{2} \right)^{-1} \quad , \quad A_c = \left(\frac{g_c^I E}{\sigma_c^2} - \frac{1}{2} \right)^{-1}$$

2.8. Homogenised masonry cell stresses.

When the elasto-plastic-damage iterative loop (Fig. 3) reach convergence on the internal variables (stresses and strains), the unknown homogenised stresses of the masonry cell can finally be easily calculated as :

(79) $$\sigma_{xx}^0 = \frac{t\left(r^{1A}\sigma_{xx}^{1A} + r^{1B}\sigma_{xx}^{1B}\right) + 2hr^b\bar{\sigma}_{xx}^b}{2\left(t+h\right)}$$

(80) $$\sigma_{yy}^0 = \frac{tr^2\sigma_{yy}^2 + lr^b\sigma_{yy}^b}{\left(t+l\right)}$$ Upper boundary

(81) $$\sigma_{xy}^0 = \frac{tr^2\sigma_{xy}^2 + lr^b\bar{\sigma}_{xy}^b}{\left(t+l\right)}$$ Upper boundary

Eq.(79) can be written for the vertical sections of the masonry cell passing through the middle of the bed joints.

2.9. Jacobian and numerical implementation

The non linear model described in previous sections has been translated in a Fortran user subroutine for a standard finite element code, the commercial package Abaqus (2007). The goal is to define the mechanical behaviour of masonry heterogeneous structure simply as a new constitutive model of an equivalent homogenised material, relating average stresses and strains in the composite material. The subroutine must update the stresses and the internal variables to their values at the end of the load increment and must provide the material Jacobian matrix $\partial\boldsymbol{\sigma}/\partial\boldsymbol{\varepsilon}$ of the mechanical model, required for the quadratic convergence of the global Newthon-Raphson method.

The tangent stiffness matrix cannot be obtained in an explicit analytical form, so an approximated direct numerical approach (forward difference derivative) has been used. If stress and strains are expressed in vector notation :

$$\mathbf{J} = \frac{\partial\boldsymbol{\sigma}}{\partial\boldsymbol{\varepsilon}} \cong \frac{\delta\boldsymbol{\sigma}}{\delta\boldsymbol{\varepsilon}} \tag{82}$$

where $\delta\boldsymbol{\varepsilon}$ is an arbitrary suitable strain increment in the neighbourhood of the updated strain value. It is noted that the proposed model is non-symmetric already in the elastic range, as the homogenized material becomes anisotropic. In addition, the adopted non-linear models provide a non-symmetric tangent stiffness model, as well known from the plasticity theory. Therefore, a non-symmetric tangent stiffness matrix was used in the Netwon-Raphson solution procedure.Eqs.(65) and (78) correlate plasticity and damage models with experimental fracture data $G_{I,II}$ through the material *specific* fracture energies $g = G/l_c$, where l_c is the characteristic internal length of fracture. As in Zucchini and Lourenço (2004) and Zucchini and Lourenço (2007) the characteristic lengths are assumed to be the

component thickness perpendicular to the expected crack direction. The main advantage of the implementation of an homogenisation approach in a f.e. program is the possibility to discretize masonry structures with fewer finite elements, larger than a single periodic cell. In this case the characteristic lengths must be scaled appropriately with the dimensions of a rectangular finite element ($\Delta X, \Delta Y$) :

(83) $$l_c = \frac{t\Delta Y}{2(t+h)}$$ bed joints

(84) $$l_c = \frac{t\Delta X}{(t+l)}$$ head joints

(85) $$l_c = \frac{l\Delta X}{(t+l)}$$ brick

3. Validation

The mechanical model proposed in this paper is validated by a comparison with numerical and experimental results available in the literature. Tests on shear masonry walls have been carried out by Raijmakers and Vermeltfoort (1992) and by Vermeltfoort and Raijmakers (1993) in the frame of the CUR project (1997). The shear walls have dimensions 990x1000 mm^2 and are build with 18 courses, of which 16 courses are active and 2 courses are clamped in steel beams, Fig. 6. The walls are made of wire-cut solid clay bricks with dimensions 210x52x100 mm^3 and 10 mm thick mortar joints. Different vertical precompression uniformly distributed loads p are applied to the walls, before a horizontal load is monotonically increased under top displacement control in a confined way, i.e. keeping the bottom and top boundaries horizontal and precluding any vertical movement. The experimental tests considered in this paper are the solid walls identified as J4D and J5D, with p=0.30 MPa, J6D (p=1.21 MPa) and J7D (p=2.12

MPa). The results of a detailed finite element analysis of these walls with an accurate composite interface model are available in Lourenço and Rots (1997).

The f.e. mesh used in this work for the analyses with the homogenisation model is an 8x8 mesh (bold dashed lines in Fig. 6a) of plane stress linear (4-noded) elements with full integration. The homogenisation model is completely defined by the material parameters summarized in Table 1 and taken from Lourenço and Rots (1997) with the exception of G_c^I, which is not available. The parameter α in Eq.(72), which controls the contribution of the shear stress to compressive mortar failure, is taken equal to 9.0. Such value is adopted, as in the simulation with the composite interface model (Lourenço and Rots, 1997), because the mortar compression damage model aims at including also some transverse cracking in the unit, not taken into account in the present damage model of the brick. To simulate the stiff upper (lower) steel beam, the top (bottom) boundary nodes of the mesh are constrained to have the same horizontal and vertical displacements. Simulation of masonry behaviour up to failure, with hardening-softening of the materials and possible local or global instabilities, is a highly non linear problem, which makes convergence of the the f.e. analysis difficult to reach. To overcome this problem, the line search algorithm, the unsymmetrical solution scheme and the stabilization option have been activated in the f.e. solver. With the stabilization option the solver adds artificial damping to the model through fictitious viscous forces, keeping the ratio of the dissipated strain energy to the total strain energy lower than a chosen tolerance ($2x10^{-3}$).

Deleted: (72

The final experimental crack pattern for wall J4D is shown in Fig. 6c. The behaviour of the other walls is similar. In wall J4D (lower precompression vertical load) horizontal tensile cracks develop at the bottom and top of the wall at an early loading stage but, finally, a diagonal stepped crack leads to collapse,

simultaneously with cracks in the bricks and crushing of the compressed toes. This behaviour of the wall is well captured by the numerical analysis with the detailed composite interface model (Lourenço and Rots, 1997) : after the horizontal tensile cracks, a stepped diagonal crack starts in the middle of the wall and is accompanied by initiation of cracks in the bricks. Under increasing deformation, the crack progresses in the direction of the supports and, finally, a collapse mechanism is formed with crushing of the compressed toes and a complete diagonal crack through joints and bricks (Fig. 7a).

The results of the f.e. simulation of wall J4D with the present homogenisation model are given in Fig. 7b and Fig. 8: the distribution of the normal strains ε_{xx} and ε_{yy} at a displacement d=3.1 mm shows the formation of a complete diagonal crack with the maximum opening in the centre of the wall. This crack is due to tensile failure of bed and head joints starting from the centre of the wall. Two horizontal tensile cracks and two compressed toes are also clearly visible in the corners of the wall in Fig. 8b. The comparison of the minimum principal stress at collapse, between the composite interface model and the homogenisation model, is given in Fig. 7. The distributions of the internal forces at collapse are similar, with the formation of two compressive struts, one of each side of the diagonal crack, in both cases. The apparent difference in the scales of the results is only due to the f.e. graphic program, which in the homogenisation model averages the stress in the nodes between concurring elements. The unaveraged extrapolated minimum principal stresses obtained with the homogenisation model actually range between –11.1 and +0.50 MPa, in good agreement with the interface model range.

In the experiments both horizontal and vertical reactions were measured and numerical results of the reaction loads, with the interface model, are available in

Lourenço (1996). An overall comparison between numerical and experimental load-displacement curves is shown in Fig. 9, which gives the horizontal reactions in tests J4D, J6D, J7D and the vertical reaction in test J4D respectively. The homogenisation model collapse loads are in reasonable agreement with both experimental and interface model results. In test J7D both numerical models overestimate the collapse load, with the homogenisation model closer to the interface model result.

4. Conclusions

In previous research, a micro-mechanical model for masonry homogenisation in the non linear domain has been proposed and validated for a single quarter cell under normal loads. In the micro-mechanical model, suitable elastic deformation mechanisms are coupled with damage and plasticity models to simulate the behaviour and the degradation of the material properties of a masonry cell during the loading path up to failure. In this work the previous model is improved, extended to a full periodic cell, implemented in a commercial finite element program and validated by comparison with available numerical and experimental results of a masonry wall under mixed in-plane loads.

The aim of the work is to demonstrate that the qualitative mechanical behaviour of a masonry wall under in-plane loads, up to collapse, can be captured by means of the proposed micro-mechanical homogenisation model. The main concern is to show the capability of the core of the homogenisation model, i.e. the set of elastic micro-mechanical deformation mechanisms, to reproduce the overall cell behaviour as predicted by detailed finite element models. For this reason, the damage and plasticity models in the homogenisation approach have been chosen

as similar as possible to those adopted in the interface model, to avoid other possible discrepancy sources.

The numerical simulations of TU Eindhoven shear walls show that the finite element analyses with a homogenised material, defined by the micro-mechanical model, and a coarse mesh provides global results in acceptable agreement with both a much more detailed plastic finite element calculation and the experimental results. The simulation captures also the basic features (tensile and compression cracks in the corners, diagonal crack, compression crushing) of the wall deformation up to the final collapse. Implementation of the method seems promising in reducing the computational effort required to analyze complex masonry structures and its implementation in a standard finite element program opens the door to larger investigation possibilities.

5. References

Abaqus, 2007, Abaqus standard reference manuals, version 6.7, Simulia, Providence, RI, USA.

Calderini, C, Lagomarsino, S, 2006. A micromechanical inelastic model for historical masonry. Journal of Earthquake Engineering, 10(4): 453-479.

CUR, 1997. Structural masonry: An experimental/numerical basis for practical design rules. Rots JG (ed). Balkema : Rotterdam.

Ju, JW, 1989. On energy-based coupled elasto-plastic damage theories: constitutive modeling and computational aspects. International Journal of Solids and Structures, 25, 803-833.

Lourenço, PB, 1996. Computational Strategies for Masonry Structures. PhD Thesis, Delft University of Technology. Available from www.civil.uminho.pt/masonry

Lourenço, PB, 2002. Computations of historical masonry constructions, Progress in Structural Engineering and Materials, 4, 301-319.

Lourenço, PB, Milani, G, Tralli, A, Zucchini, A, 2007. Analysis of masonry structures: review of and recent trends of homogenisation techniques, Canadian Journal of Civil Engineering, 34, 1443-1457.

Lourenço, PB, Ramos, LF, 2004. Characterization of the cyclic behavior of dry masonry joints. Journal of Structural Engineering, ASCE, 130, 779-786.

Lourenço, PB, Rots, JG, 1997. Multisurface interface model for the analysis of masonry structures. J. Engineering Mechanics, ASCE, 123, 660-668.

Massart, TJ, Peerlings, RHJ, and Geers, MGD. 2004. Mesoscopic modeling of failure and damage-induced anisotropy in brick masonry. European Journal of Mechanics A/Solids, 23: 719-735

Mazars, J, Pijaudier-Cabot, G., 1989. Continuum damage theory - application to concrete. Journal of Engineering Mechanics, 115,345-365.

Milani, G, Lourenço, PB, Tralli, A, 2006. Homogenised limit analysis of masonry walls. Part I: Failure surfaces, Computers & Structures, 84(3-4), 166-180.

Peerlings, RHJ, de Borst, R, Brekelmans, WAM, Geers, MGD, 1998. Gradient-enhanced damage modelling of concrete fracture. Mechanics of cohesive-frictional materials, 3, 323-342.

Shieh-Beygia, B, Pietruszczak, S, 2008. Numerical analysis of structural masonry: mesoscale approach, Computers & Structures, in press.

Raijmakers, TMJ, Vermeltfoort ATh, 1992. Deformation controlled tets in masonry shear walls (in dutch). Report B-92-1156, TNO-Bouw, Delft, The

Netherlands.

Vasconcelos, G, 2005. Experimental investigations on the mechanics of stone masonry: characterization of granites and behavior of ancient masonry shear walls. PhD Thesis, University of Minho.

Vermeltfoort, ATh, Raijmakers, TMJ, 1993. Deformation controlled tets in masonry shear walls, Part 2 (in dutch). Report TUE/BKO/93.08, Eindhoven University of Technology, Eindhoven, The Netherlands.

Zucchini A, Lourenço PB, 2002. A micro-mechanical model for the homogenisation of masonry. International Journal of Solids and Structures, 39, 3233–3255.

Zucchini, A, Lourenço, PB, 2004. A coupled homogenisation-damage model for masonry cracking. Computer and Structures, 82, 917–929.

Zucchini, A, Lourenço, PB, 2007. Mechanics of Masonry in Compression: Results from a Homogenisation Approach. Computer and Structures, 85, 193-204.

Figure Captions

Fig. 1

Basic cell for masonry and homogenisation process.

Fig. 2

Adopted geometry symbols.

Fig. 3

Iterative procedure for the homogenisation of a non-linear masonry cell, with damage and plastic behaviour, under a strain load increment.

Fig. 4

Full cell antisymmetric deformation mechanism under vertical load.

Fig. 5

Full cell antisymmetric deformation mechanism under shear : (a) in y ; (b) in x.

Fig. 6

TU Eindhoven shear walls JD : (a) vertical precompression; (b) horizontal loading under displacement control; (c) experimental crack pattern for test J4D.

Fig. 7

Minimum principal stresses for test J4D : (a) interface model at d=4.0 mm; (b) homogenisation model at d=3.1 mm.

Fig. 8

Normal strains by homogenisation model in test J4D at d=3.1 mm : (a) ε_{xx} ; (b) ε_{yy}.

Fig. 9

Comparison between experimenta results, interface model and homogenisation model : (a) horizontal force vs. displacement for wall J4D; (b) horizontal force vs. displacement for wall J6D; (c) horizontal force vs. displacement for wall J7D; (d) vertical force vs. displacement for wall J4D.

Table Caption

Table 1.

Shear walls JD : Mechanical properties of the masonry components.

Table(s)

Table 1

	p MPa	E GPa	ν	σ_t MPa	G_t^I J/m^2	σ_c MPa	G_c^I J/m^2	c_0 MPa	G^{II} J/m^2	ϕ_f °	ϕ_d °
Masonry	0.30 1.21 2.12	0.8 1.0 0.8	0.15	0.25 0.16 0.16	18 12 12	10.5 11.5 11.5	2800	0.35 0.224 0.224	125 50 50	36.9	0
Brick		16.7	0.15	2	80.0	-	-	-	-	10	5

Figure(s)

Figure 1

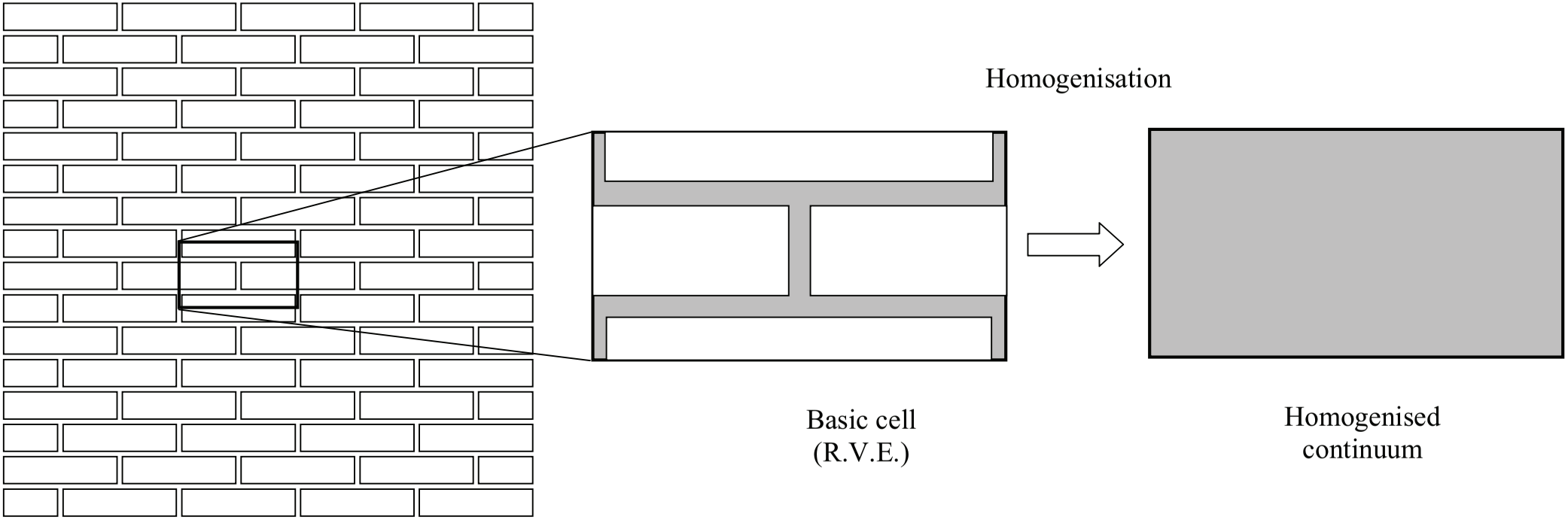

Figure 2

1A,1B : Bed Joints
2 : Head Joint
3 : Cross Joint
b :Unit

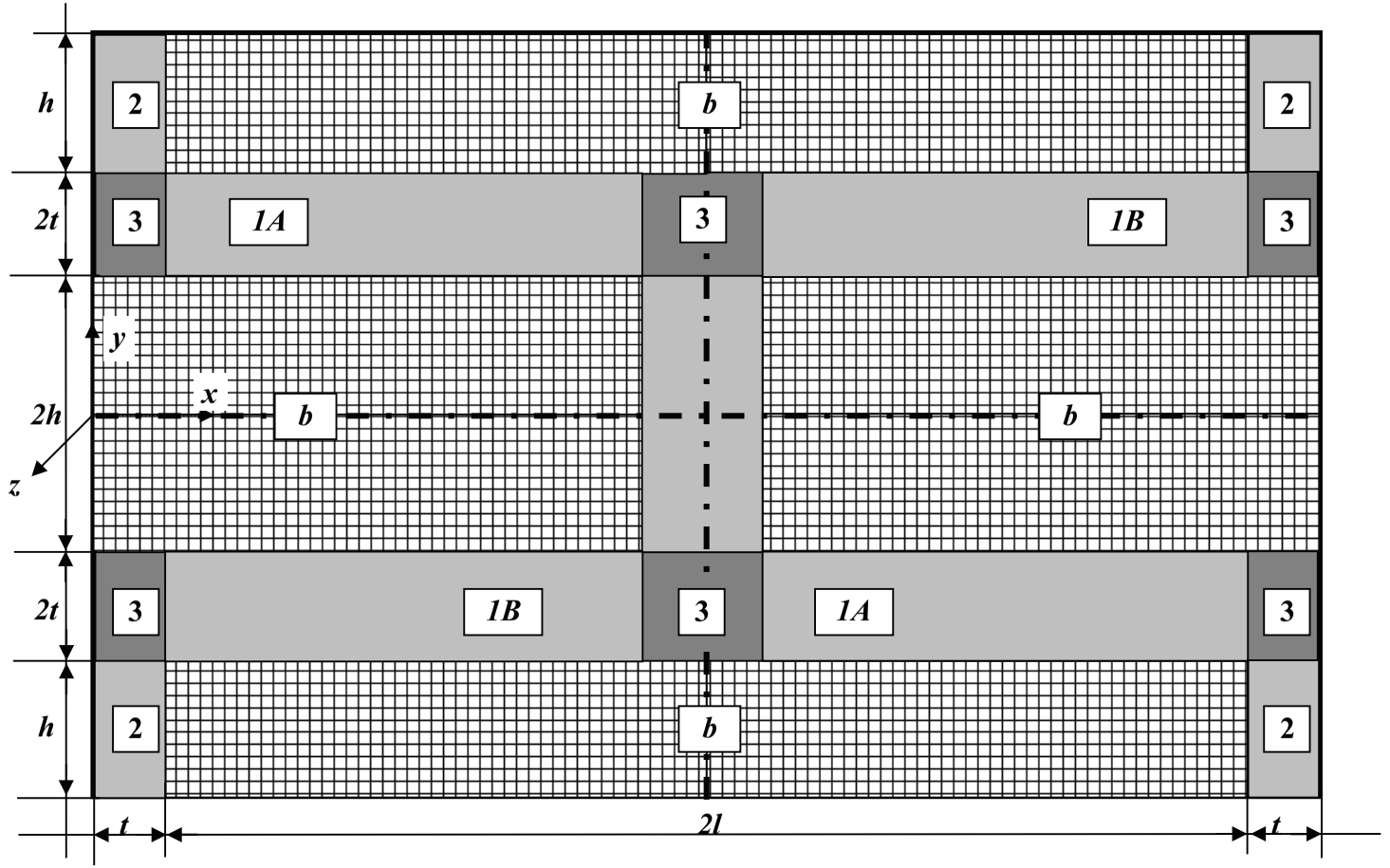

Figure 3

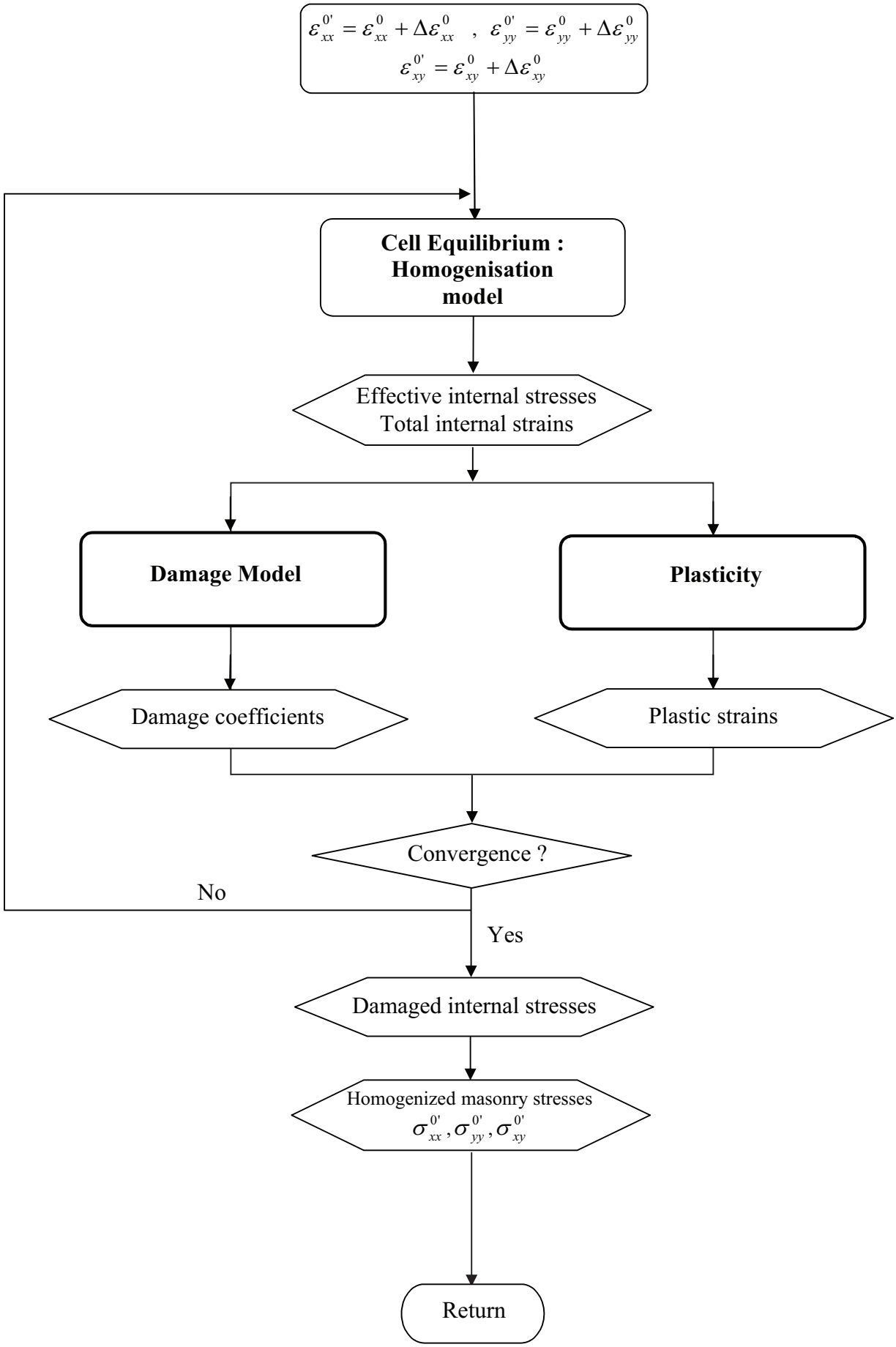
$\varepsilon_{xx}^{0'} = \varepsilon_{xx}^{0} + \Delta\varepsilon_{xx}^{0}$, $\varepsilon_{yy}^{0'} = \varepsilon_{yy}^{0} + \Delta\varepsilon_{yy}^{0}$
$\varepsilon_{xy}^{0'} = \varepsilon_{xy}^{0} + \Delta\varepsilon_{xy}^{0}$
Cell Equilibrium : Homogenisation model
Effective internal stresses
Total internal strains
Damage Model
Plasticity
Damage coefficients
Plastic strains
Convergence ?
No
Yes
Damaged internal stresses
Homogenized masonry stresses
$\sigma_{xx}^{0'}, \sigma_{yy}^{0'}, \sigma_{xy}^{0'}$
Return

Figure 4

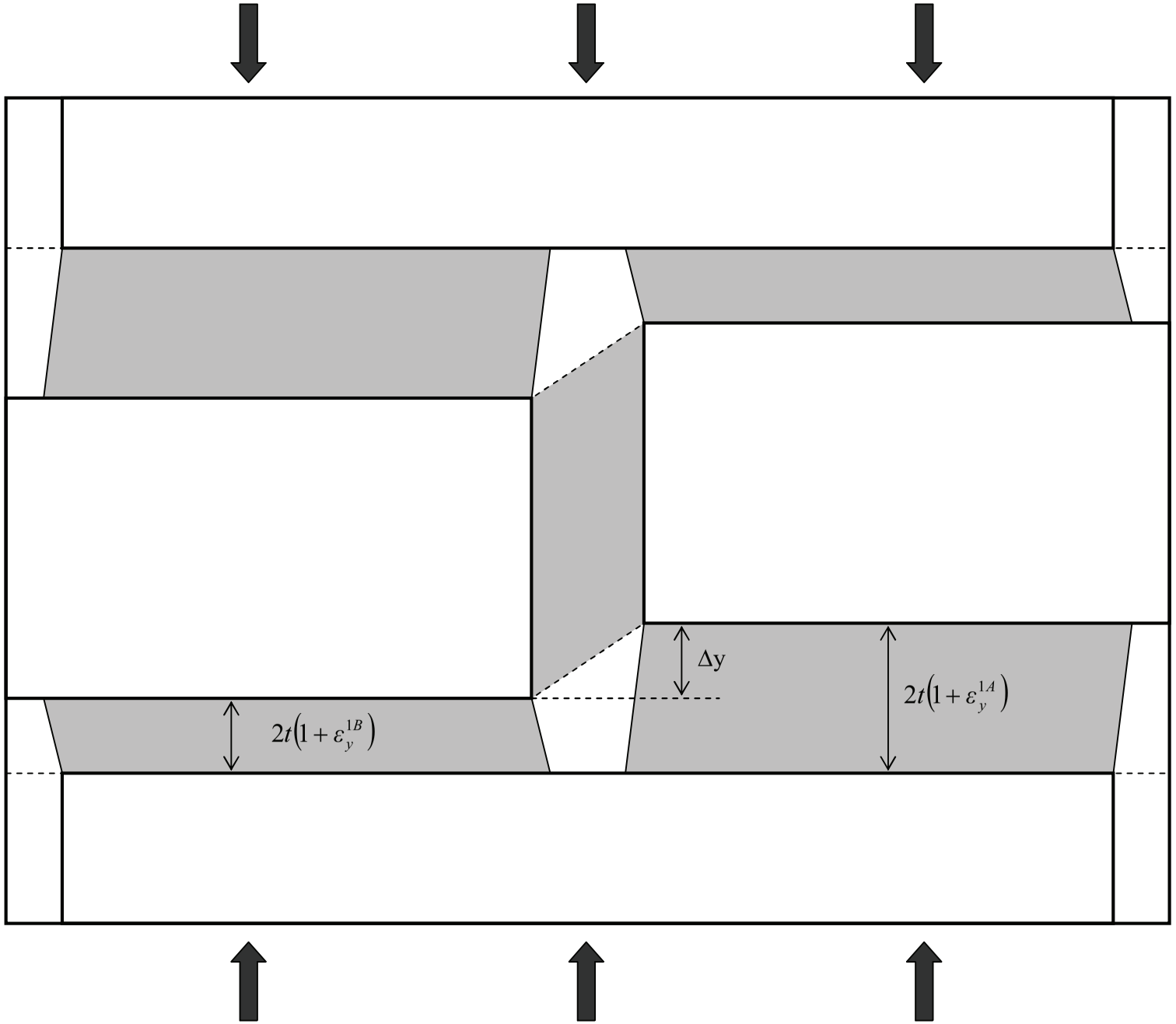
Δy
$2t\left(1+\varepsilon_y^{1B}\right)$
$2t\left(1+\varepsilon_y^{1A}\right)$

Figure 5

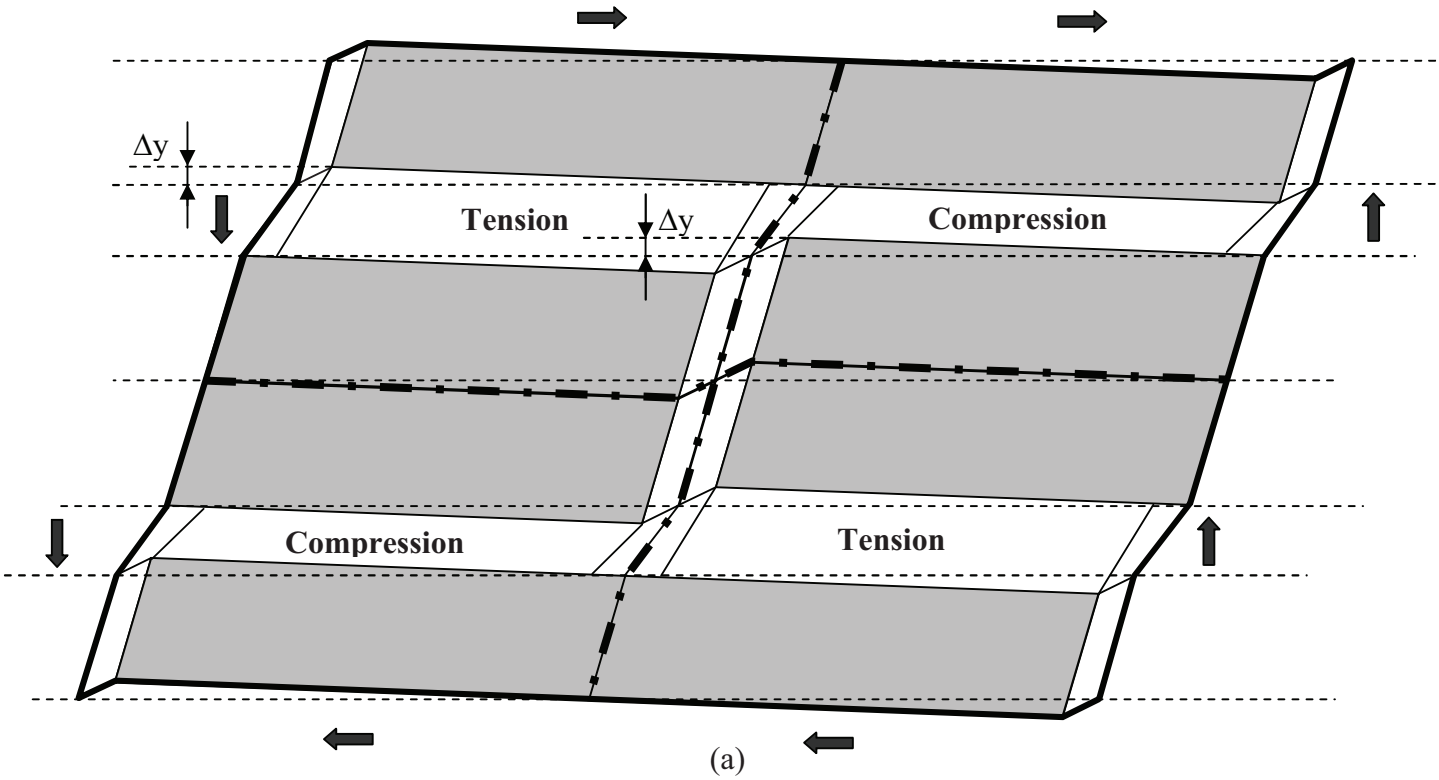
Δy
Tension
Δy
Compression
Compression
Tension

(a)

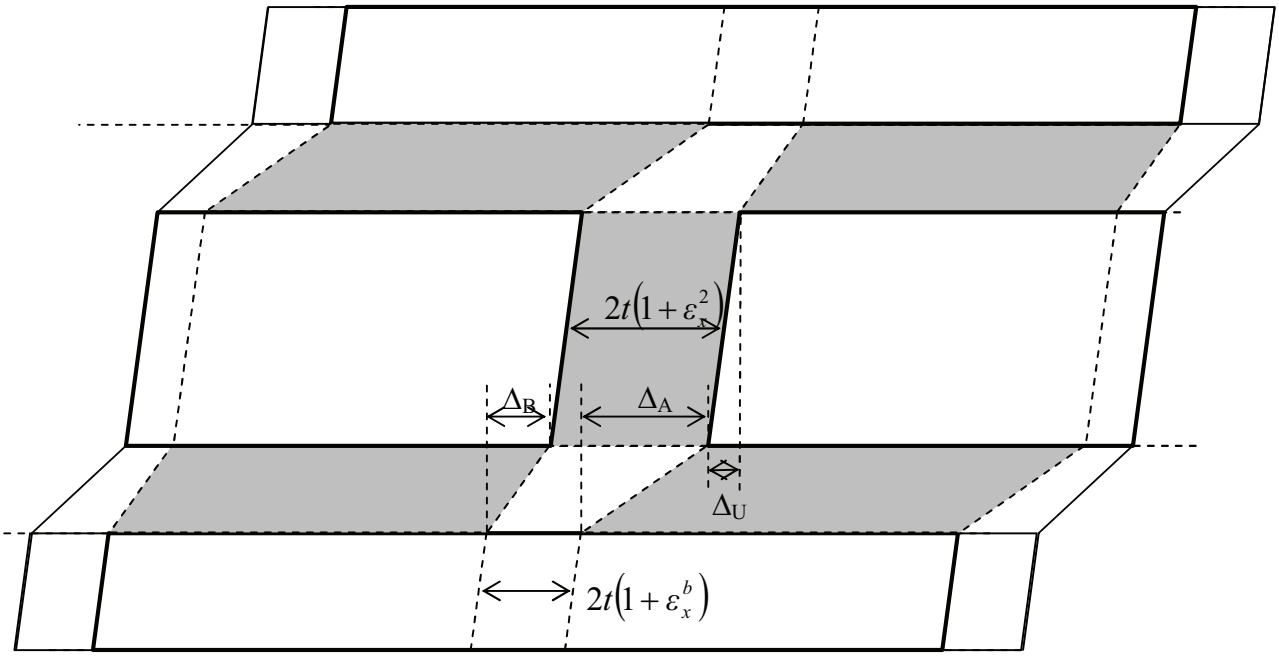
$2t\left(1+\varepsilon^2\right)$
Δ_B
Δ_A
Δ_U
$2t\left(1+\varepsilon_x^b\right)$

(b)

Figure 6

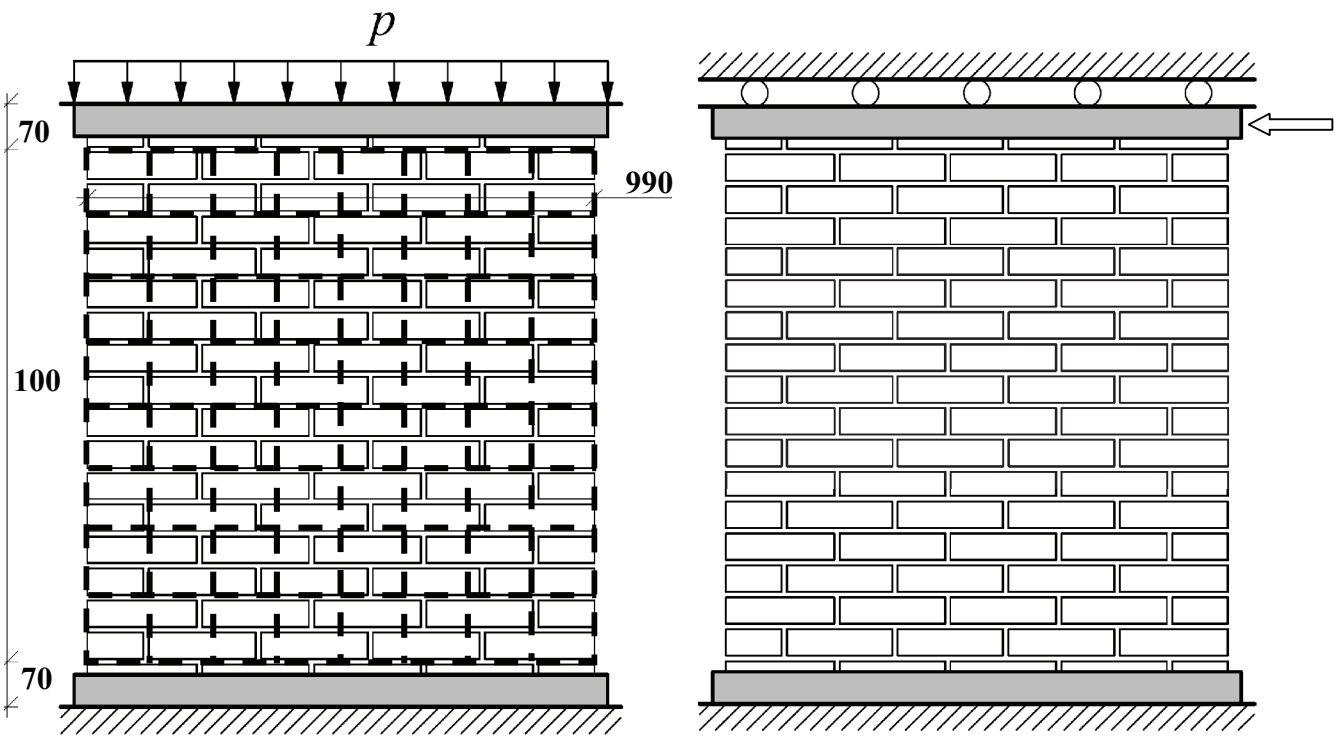

(a) (b)

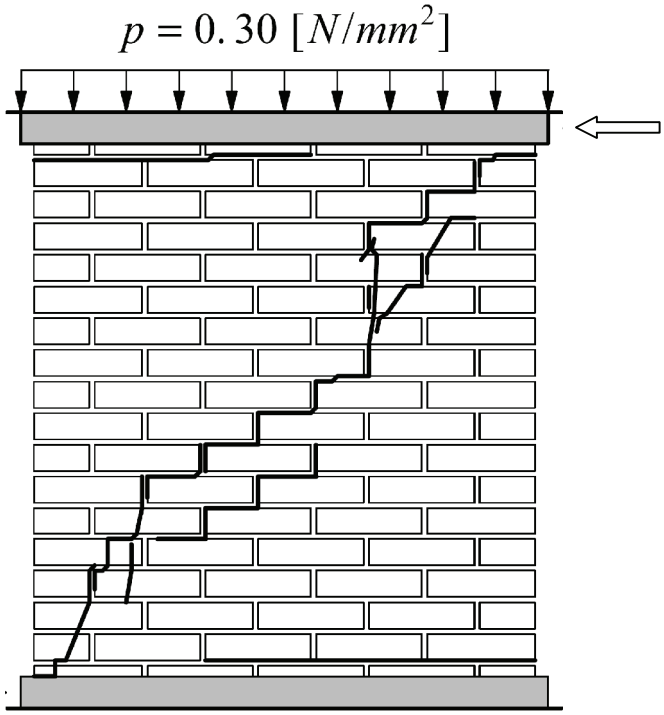

Wall J4D

(c)

Figure 7

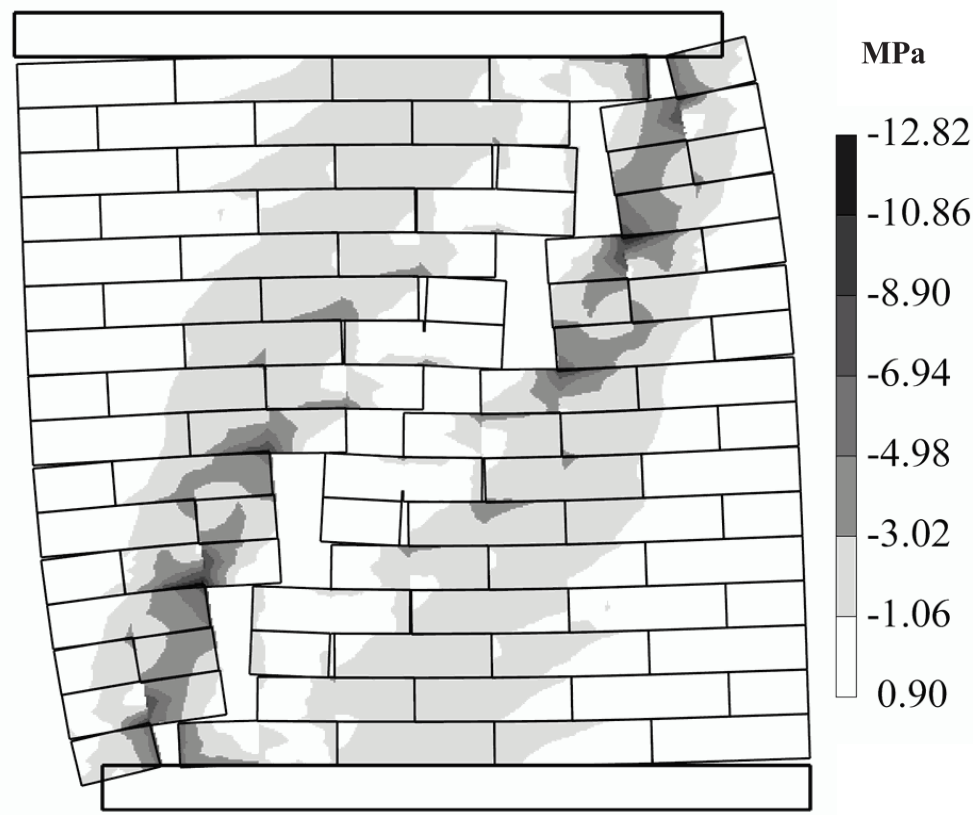
MPa
-12.82
-10.86
-8.90
-6.94
-4.98
-3.02
-1.06
0.90

(a)

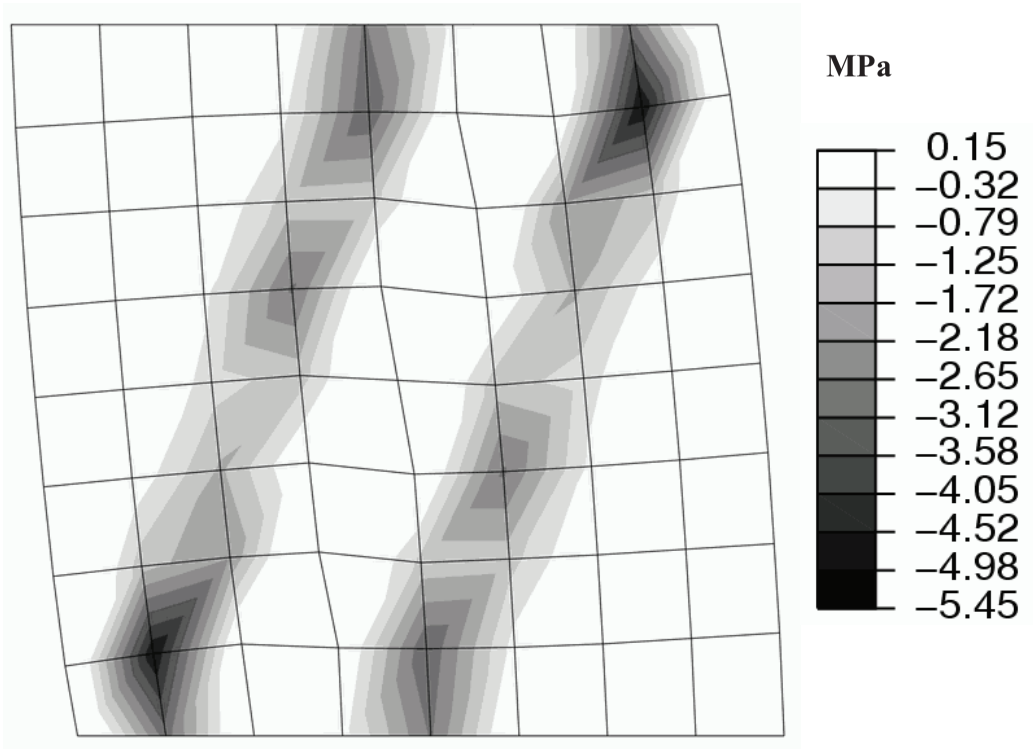
MPa
0.15
−0.32
−0.79
−1.25
−1.72
−2.18
−2.65
−3.12
−3.58
−4.05
−4.52
−4.98
−5.45

(b)

Figure 8

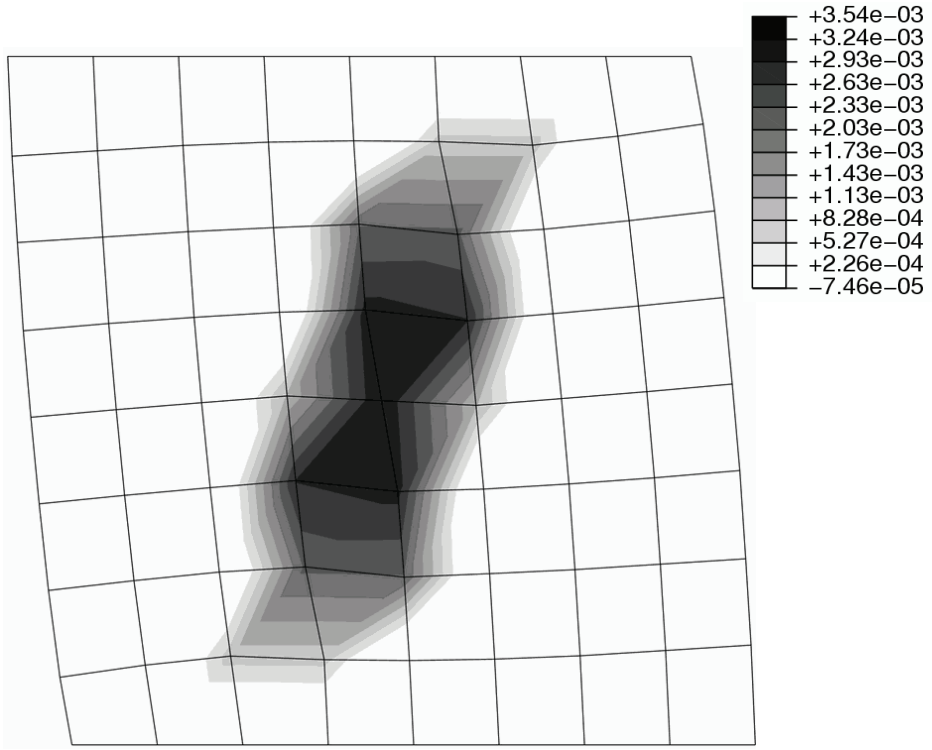
+3.54e−03
+3.24e−03
+2.93e−03
+2.63e−03
+2.33e−03
+2.03e−03
+1.73e−03
+1.43e−03
+1.13e−03
+8.28e−04
+5.27e−04
+2.26e−04
−7.46e−05

(a)

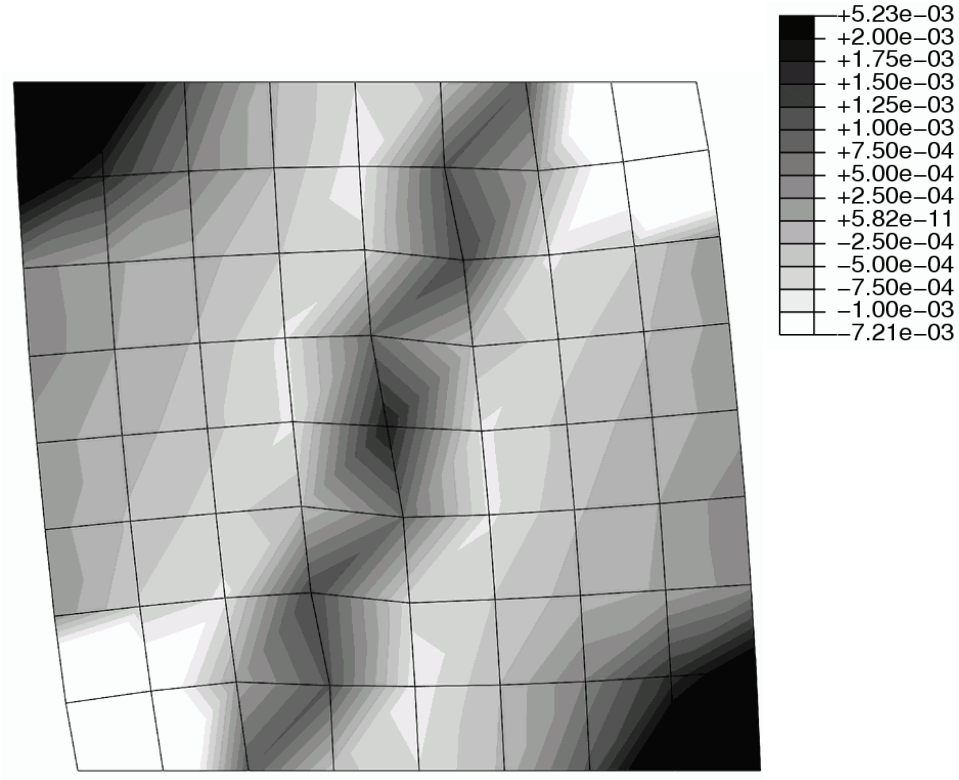
+5.23e−03
+2.00e−03
+1.75e−03
+1.50e−03
+1.25e−03
+1.00e−03
+7.50e−04
+5.00e−04
+2.50e−04
+5.82e−11
−2.50e−04
−5.00e−04
−7.50e−04
−1.00e−03
−7.21e−03

(b)

Figure 9

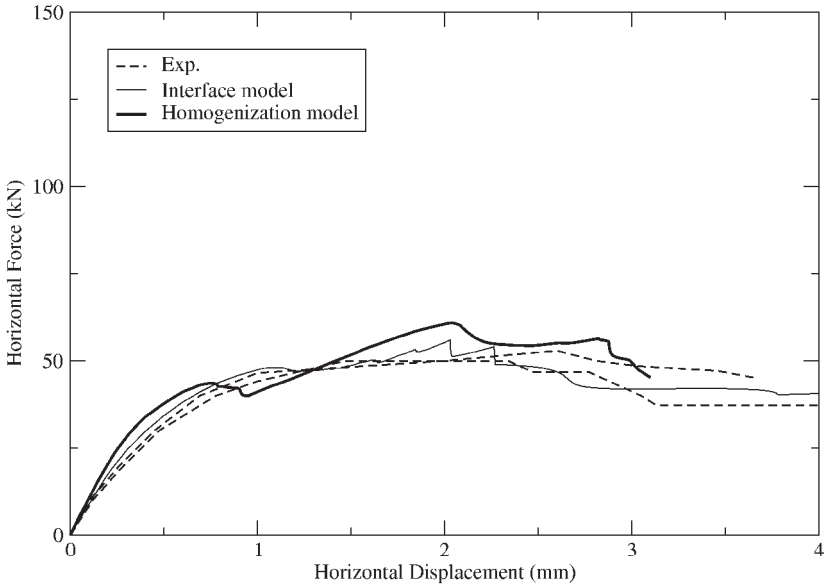

(a)

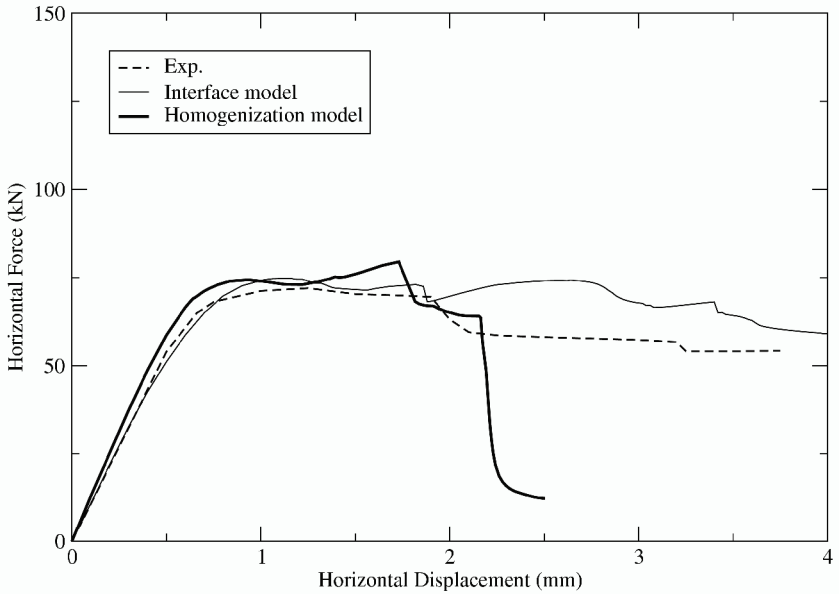

(b)

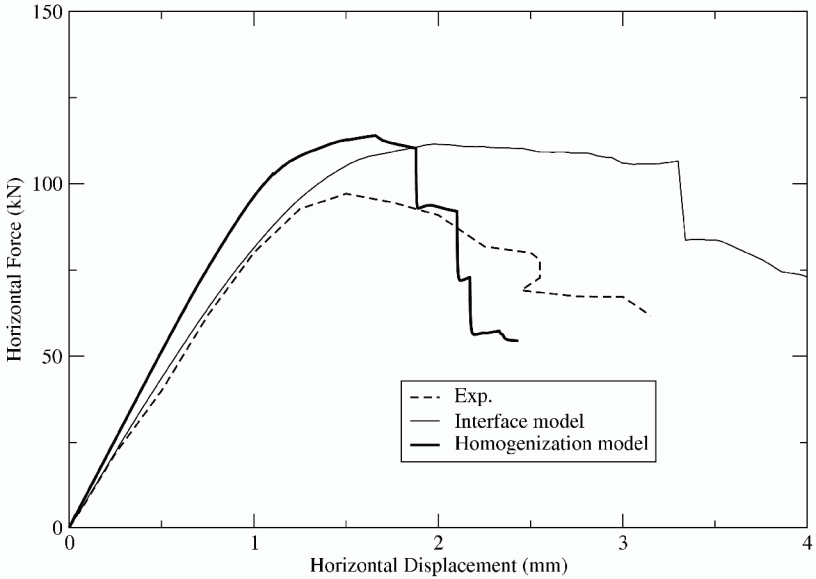

(c)

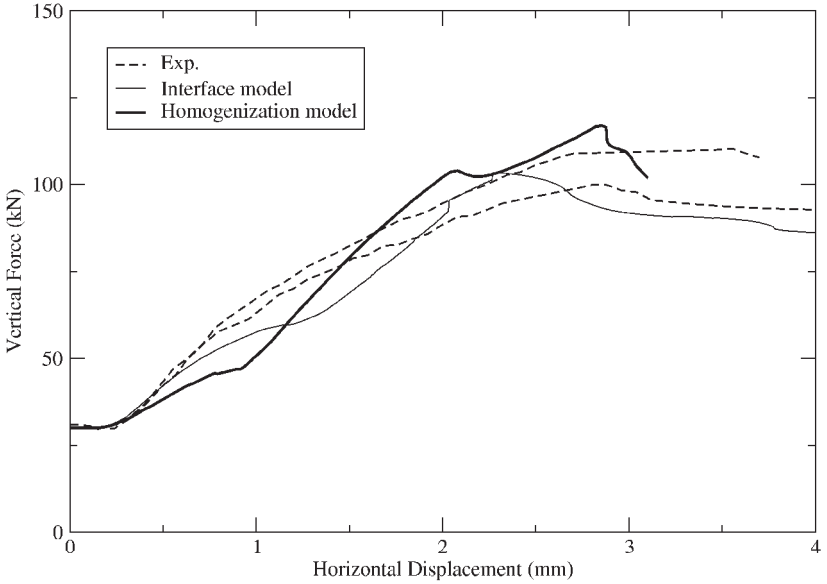

(d)